Porous GaN and high-κ MgO-GaN MOS diode layers grown in a single step on silicon

O. V. Bilousov[1], J. J. Carvajal[1*], A. Vilalta-Clemente[3], P. Ruterana[3], F. Díaz[1], M. Aguiló[1], and C. O'Dwyer[2,4]*

[1] *Física i Cristallografia de Materials i Nanomaterials (FiCMA-FiCNA) and EMaS, Universitat Rovira i Virgili (URV), Marcellí Domingo s/n, E-43007 Spain*

[2] *Department of Chemistry, University College Cork, Cork, Ireland*

[3] *CIMAP, UMR 6252 CNRS-ENSICAEN-CEA-UCBN, 6 Boulevard du Maréchal Juin, 14050 Caen Cedex, France*

[4] *Micro & Nanoelectronics Centre, Tyndall National Institute, Lee Maltings, Cork, Ireland*

**corresponding authors: c.odwyer@ucc.ie; joanjosep.carvajal@urv.cat*

Porous GaN polycrystalline layers with n-type conduction characteristics were catalytically grown from Mg films formed by decomposition of a Mg_2N_3 precursor typically employed for activating p-type conduction in GaN. After exposure to oxygen, the Mg film oxidized to a polycrystalline high-κ oxide between the ohmic alloy interlayer contact and the porous GaN, while maintaining a clean interface. Electrical measurements on devices coupled to composition analysis and electron microscopy of the component layers confirm that a MOS-type porous GaN diode on silicon can be formed by chemical vapour deposition in a single growth regime.

Introduction

Gallium nitride (GaN) and its alloys have proven their importance as wide band-gap semiconductors for a number of applications in electronics and optoelectronics [1]. In its porous and nanostructured forms, GaN[2], InGaN[3] and InN[4] have received particular interest in the last decade due to beneficial optical and electronic properties for optoelectronics, gas sensors with high sensitivity, light-emitting diodes (LEDs) with high light extraction efficiency[5], wide-band gap biosensors[6-7] and high electron mobility transistors for high frequency and high power devices. Nanoscale analogs of III-N materials have been investigated to probe exotic optical and high mobility transport[8] effects particularly for photonics applications[9-10]. The wide bandgap of GaN can minimize the generation of charge carriers due to undesirable background optical or thermal excitations, but also allow for electroluminescent color-tuning from the ultraviolet to the infra-red in multiple-quantum well (MQW)[11] or nanowire[12] heterostructures.

Porous semiconductor materials such as Si[13-15], III-Vs[16] and also GaN[17-18], have been typically fabricated by (photo)electrochemical and chemical etching[19] methods, giving textured surfaces as a result of pore coalescence and variations in etch rates for extended etching times. Controlling the degree of porosity in a functional layer of GaN is more difficult that top-down etching to relieve array of nanostructures for example. Alternative methods to introduce porosity in high quality, doped GaN is advantageous for several high surface area, chemically stable applications requiring wide band gaps, such as biosensors with optically active regions. Due to the wide-bandgap nature of the material (3.5 eV for GaN compared to 1.12 eV for Si), it is extremely stable to temperature increase, and electronic devices can be operated at temperatures up to 500ºC. Usefully, there is no effective uniform wet chemical etchant for GaN, making it chemically stable in almost any liquid environment.

In recent years, a considerable research and development effort into chemical and biosensors[20] was driven by a high demand for biosensors[21] that can be used in glucose monitoring, infectious diseases biomarking, and in cancer diagnosis that use capacitance and electrical properties of semiconductors[22]. Wide band gap sensors are being developed for point-of-care applications and in particular[6], transistor based sensors hold a lot of promise for application in medical science in addition to optoelectronics[23]. In transistor geometry, device physics can be married to sensor requirements to offer improvements in precision, stability, faster response times, and with high surface areas such as those provided by porous semiconductors, can be made sensitive to minute quantities of analyte[7, 24-26]. To do this, the transistors use variations in the effective barrier height caused by the material or liquid being analysed on the surface of the device. These devices are typically high electron mobility transistors (HEMTs) and benefit from a high two dimensional electron gas (2DEG) mobility and saturation velocity[27]. The conducting 2DEG channel of AlGaN/GaN HEMTs for example, is extremely sensitive to charge alteration from adsorption of analytes or species as it is designed close to the surface of the device.

Such sensors can also benefit from high surface areas of high quality GaN and related materials, but mass production would also benefit from lower cost routes to upscaled device manufacture. We previously produced porous GaN through the direct reaction of metallic Ga with NH_3 in a simple chemical vapor deposition (CVD) system on sapphire and Si substrates[28-29]. Metal catalysts are typically used to initiate growth through either a vapor-liquid-solid (VLS) or vapor-solid-solid (VSS) mechanism[30] when using molecular beam epitaxy (MBE) and chemical vapor deposition (CVD), where the catalyst can influence the growth without necessitating any secondary etching or chemical treatment after GaN growth to induce porosity.

Reports of Schottky diodes based on porous GaN have shown good performance for hydrogen gas sensing applications[31-32], and this can be extended to

three-terminal devices. In higher surface area GaN based devices, electrochemical etching techniques were used, some of which can provoke surface damage or electronic surface state variations that can lead to changes in barrier heights in some cases.

For thin-film transitors (TFTs) and metal-oxyde-semiconductor (MOS)-HEMTs, high-κ dielectrics can help reduce the operating voltage, increased drain current density and transconductance, using a high mobility 2DEG. High-κ growth with porous III-N systems has not been investigated and routes for channel dielectric Magnesium oxide (MgO) is a candidate of high-k gate dielectrics (κ = 9.4~9.8)[33] because of its good isolation[34] and chemically inert properties. Additionally, using bottom up catalytic growth processes for III-Ns, Mg precursors are typically used to create p-type conduction characteristics after lattice incorporation and thermal activation of these acceptors.

In this paper, we present a new method of fabrication of MOS diodes based on metal-catalyzed high surface area porous GaN layers with a MgO high-κ dielectric layer located in between the metallic electrode (Ga-Pt or Ga_2Au-based intermetallic Ohmic contacts) in a single bottom-up catalytic growth step. Electrical measurements demonstrate the influence of the growth mechanism so that near-ohmic contacts can be made to n-type porous GaN layers using alloyed interlayer contacts. Mg-based precursors were deposited in such a way as to seed a Mg film under the porous GaN, which was oxidatively crystallized to MgO without affecting the conduction type or composition of the GaN layer. Charge transport measurements allowed us to demonstrate the fabrication of a Ga_2Au/MgO/GaN/In-Ga high surface area MOS diode.

Experimental

Synthesis and catalyzed growth of porous GaN layer

For synthesis of porous GaN nanostructures by chemical vapor deposition (CVD) a horizontal single zone split tubular furnace Thermolyne 79300, Thermo Fisher Scientific Inc., USA with a built-in temperature controller was used. Nanoporous GaN doped with Mg was grown as micron-sized particles by the direct reaction of metallic Ga with ammonia in a tubular CVD system, using gallium metal (99.99%), ammonia (>99.98%) and Mg_3N_2 (99.5%) as the Ga, N and Mg sources, respectively. These particles were deposited on Si(100) wafers. A 20 nm layer of Au or Pt, acting as a catalyst in the reaction, was deposited on the Si substrates using a RF sputtering process (AJA International) at a power of 150 W and a pressure of 3 mTorr. The coated substrate was then placed 2 cm above the Ga source. The Mg_3N_2 powder, with a 0.025 to 1 weight ratio respect to Ga, was placed 4 cm up-stream of the Ga source. The quartz tube of the furnace was degassed to a vacuum pressure of 1×10^{-2} Torr. Afterwards, ammonia was introduced through a mass-flow controller and the furnace was heated up to the reaction temperature at a flow rate of 75 sccm and the furnace heated to the reaction temperature of 1203 K at a rate of 100 K min^{-1}. The reaction was continued at this temperature for 60 min under a constant flow of NH_3. Growth was halted by cooling to room temperature without NH_3 flow, reducing the pressure to 1×10^{-2} Torr.

Structural, morphological, and compositional characterization

X-ray diffraction (XRD) pattern in θ-2θ geometry of the as-grown sample were made using Cu Kα radiation in a Bruker-AXS D8-Discover diffractometer equipped with parallel incident beam (Göbel mirror), vertical θ-θ goniometer, XYZ motorized stage and a General Area Diffraction Detection System (GADDS) HI-STAR detector with a multiwire proportional counter of area 30 × 30 cm and 1024 × 1024 pixel density.

Samples were placed directly on the sample holder and the area of interest was selected with the aid of a video-laser focusing system. An X-ray collimator system allows to analyze areas of 500μm. The X-ray diffractometer was operated at 40 kV and 40 mA to generate Cu Kα radiation. We collected 2D XRD patterns covering a range of 2θ between 20 - 85º. Identification of the crystalline phases was achieved by comparison of the XRD diffractogram with the ICDD database using Diffrac^{plus} Evaluation software (Bruker 2007).

The nanoporous GaN microparticles deposited on the Si substrates as a porous layer were characterized morphologically using a JEOL JSM 6400 scanning electron microscope (SEM). Before observation samples were coated with a thin layer of gold with a Bal-Tec SCD004 sputterer.

The transmission electron microscopy (TEM) specimens were prepared as in the conventional way of mechanical polishing and dimpling down to a few microns followed, the electron transparency was next obtained using Ar^+ ion milling at 5 keV. The accelerating voltage was systematically decreased to 0.7 keV at the final stage in order to reduce the ion beam damage. The observations were carried out in a JEOL-2010FEG TEM operating at 200 keV, and simultaneously, energy dispersive X-ray spectroscopy (EDS) has been used to determine the local composition in the GaN(Mg).

Electrical characterization

Charge transport measurements through the porous GaN films were conducted using 2- and 4-probe measurements using a dc-voltage course and an Agilent 34401A Digital Multimeter in a Peltier cell, thermostated to 295 K in a Faraday cage. Liquid metal contacts were made using In-Ga eutectic blown into a sphere from a gold metallized short borosilicate capillary tube ensuring good wetting (several μm^2) to the rough top-surface morphology of the porous GaN and avoid electrical shorting to the

underlying metallized silicon. Resistivity values were extracted from *I-V* curves in the high bias regime (series resistance) and also from 4-point probe measurements. Diode measurements of the GaN/MgO system were made in symmetrical vertical 2-probe measurements.

Results and Discussion

Vapor-solid-solid growth of porous GaN on silicon

The growth of the GaN nanoporous particles was assisted by a solid particle through the vapour-solid-solid (VSS) mechanism, the main stages of which are: the Ga incorporation into the Au or Pt solid phase eutectic, the formation of a Ga-Au or Ga-Pt alloy, the solubilization of nitrogen in the Ga-Au(Pt) alloy, and finally the nucleation and growth of GaN[28]. Figures 1a and b confirm that the porous GaN particles grown without additional Mg vapor have a characteristic morphology consisting of faceted hourglass crystals with a mean size of ~1.5 μm. Crystal growth occurs progressively on the surface with individual crystals ripening until a layer of porous GaN microparticles in the form of single crystal truncated bipyramids[35], covers the surface as a connected porous layer, confirmed with time-resolved focused ion beam (FIB) based tomography[36].

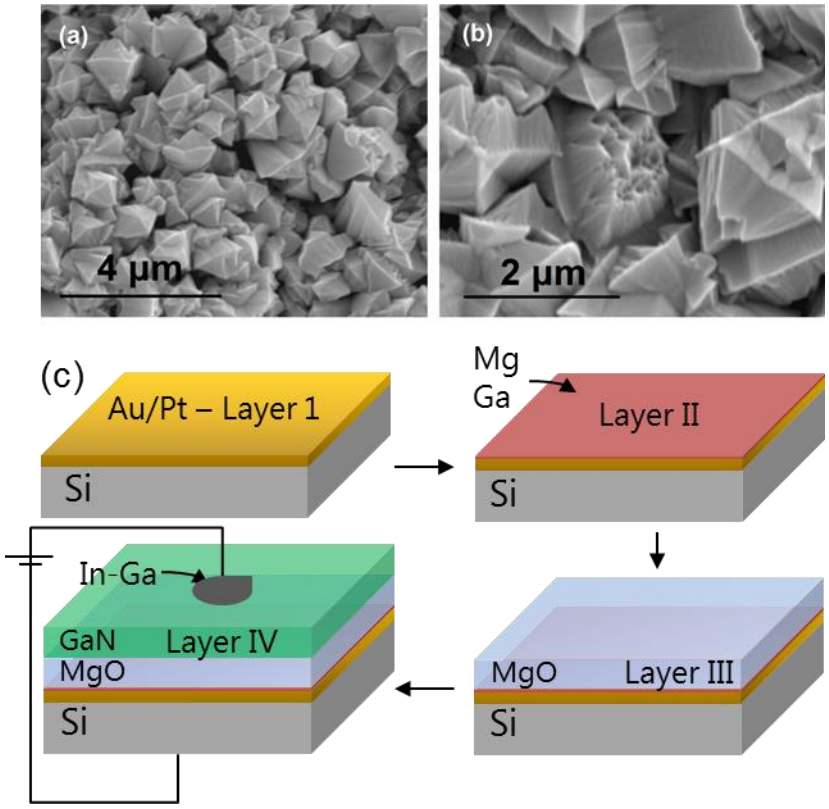

FIG 1. SEM image of porous GaN particles grown on Si (100) substrates coated with (a) 20 nm film of Au and (b) 20 nm film of Pt. (c) Mechanism of the MgO/GaN layers of the MOS diode by subsequent catalytic VSS growth during CVD.

Using Mg_3N_2, typically used for Mg doping of GaN, a layer of crystalline MgO is formed between the silicon surface and the porous GaN, depending on the initial concentration of the Mg precursor used. Two different Mg_3N_2 concentrations, 0.015 and 0.025 weight ratio respect to Ga were used. When a concentration of 0.015 was used, Mg doped porous GaN was formed[29]. Instead, for a concentration of $Mg_3N0.025$ Figure 2 shows the XRD pattern for the resulting multilayer deposition. The XRD pattern shown in Fig. 2a for MgO/GaN grown on Au-coated Si substrates, confirms crystalline wurtzite GaN growth with a predominant diffraction intensity from low-index crystal facets. The uniform intensity of the Debye rings (along the curved ring portions in Fig. 2a) confirms that there is no texturation of the layer of porous crystals, as confirmed by the SEM images shown in Figs 2b and 2d.

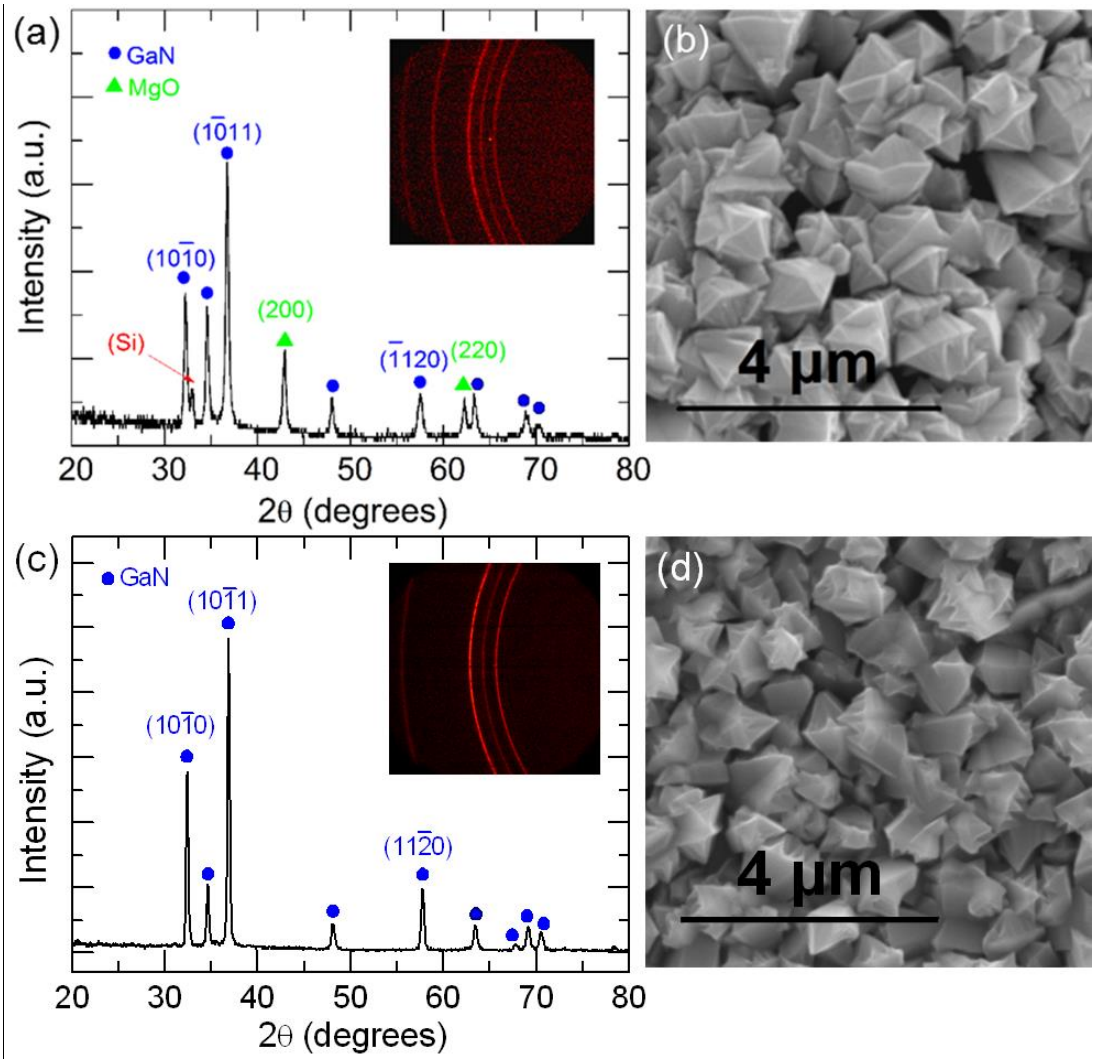

FIG 2. (a) XRD pattern for porous crystalline wurtzite GaN (P63*mc*) grown on Si(100) using a high concentration of Mg_3N_2, with inset of Debye rings. The Si(400) diffraction peak has been excluded to avoid intensity saturation. (b) SEM image of the Mg-catalyzed porous GaN grown on Si. (c) XRD pattern for porous crystalline wurtzite GaN (P63*mc*) grown on Si(100) using a low concentration of Mg_3N_2 , with inset of Debye rings. (d) SEM image of the Au-catalyzed Mg-doped porous GaN grown on Si.

We find that the deposit formed with a higher concentration of Mg_3N_2 also contains crystalline MgO, oxidatively crystallized from the Mg presence during incorporation at the growth stage of the porous GaN. The porous GaN single crystals formed in both cases are identical to those grown in the absence of the Mg precursor, and they also retain their unintentionally n-doped conduction since we did not anneal this sample to activate the p-type conduction.

In GaN nitride thin films, TEM investigations have pointed out that they can contain numerous crystallographic defects such as dislocations[37,38], inversion domains[39], basal[40] and/or prismatic stacking faults[41]. These defects form due to the large lattice and thermal mismatches which exist between GaN and the most used substrates such as sapphire[42], silicon carbide[37] or silicon[43], when the growth is carried out by MBE or metalorganic vapor phase epitaxy (MOVPE). In such instances the layers are almost monocrystalline with very highly texture domains and XRD show in plane or out of plane full width half maxima in the range of 200-300", but they also may exhibit high angle grain boundaries[44]. In our instance, the aim was to fabricate porous films and this is confirmed by the TEM analysis, which shows that the polycrystalline MgO is located under the porous GaN, in spite of being present at initial stages of the seeding mediated growth of the GaN itself. The high quantities of the Mg-containing precursors preferentially form this layer rather than doping the GaN lattice. This is in contrast with what has been observed when a smaller amount of Mg_3N_2 is used, in which case, only the polycrystalline layer of porous GaN is observed. Mg is detected in those GaN microcrystals with a tendency to have a higher Mg concentration in the crystals deposited in the latter stages and that are located at the top of the polycrystalline layer. As can be seen in Figure 3a, the porous GaN layer doped with Mg grown on a Si(100) substrate and obtained with a high concentration of Mg_3N_2, exhibits typically four different regions. EDS analysis was used to estimate the Mg content as indicated in Fig. 3a for 12 positions and Table 1. The four regions are characterized by changes in contrast which may be related to the variable Mg content (and thus scattering) in each of the marked regions. Region I corresponds to the Si substrate. In Region II, around point 1, there is a good adhesion to the Si, and the layer has a dark contrast, with a Ga content of 26.7% and Mg content of 73.3%. However, the phase formed in this region does not exhibit diffraction as an intermetallic crystal, and, therefore, it likely corresponds to a Mg-Ga alloy as is the

case with Ga-Pt reactions during GaN growth[28]. In region III (points 2 to 4), the contrast is very light, agreeing with the low (~1.5-3 %) measured content in Ga and the ~97-98 % of Mg which indicates that a new phase rich in Mg is formed, and as oxygen was also detected in our EDS analysis, this phase most probably corresponds to an (Mg-O) oxide. The area exhibits very poor crystalline state as well as large porosity, which is in agreement with the light contrast in this bright field micrograph; its thickness is ~1 μm, although with a large roughness at its top, as well as at the bottom. Towards the surface, region IV (points 5-12) is made of a polycrystalline phase which is rich in Ga (90.5-97.8 %), while the Mg content remains ~7.9-11.7% from grain to grain. This area corresponds to Mg-doped GaN made of individual grains with a mean thickness of ~0.5 μm for each of them. A close examination shows that the crystallographic relationships between these grains are very random, with no specific orientation connection, and even spacing as can be seen in position 6 and 9 in Figure 3a. Therefore, this doped GaN top layer is also porous. TEM energy dispersive X-ray analysis, shown in Fig. 3a, confirms the interfacial location of the MgO between the silicon substrate/intermetallic seed layer, and the porous GaN at the surface.

When the GaN layer was grown using a low concentration of Mg_3N_2 (Fig. 3b) only two regions have been observed. Region I corresponds to the Si substrate and Region II, totally detached from the Si substrate, corresponds to Mg-doped GaN, with a thickness of ~4.5 μm, substantially thicker than that obtained when a high concentration of Mg_3N_2 has been used. As can be seen, this layer is also porous, with more or less elongated and good quality crystallites throughout the layer thickness. The EDS analysis corresponding to 10 separate locations of this sample, also listed in Table 1, indicates that the content of Mg present a slight increase towards the layer surface.

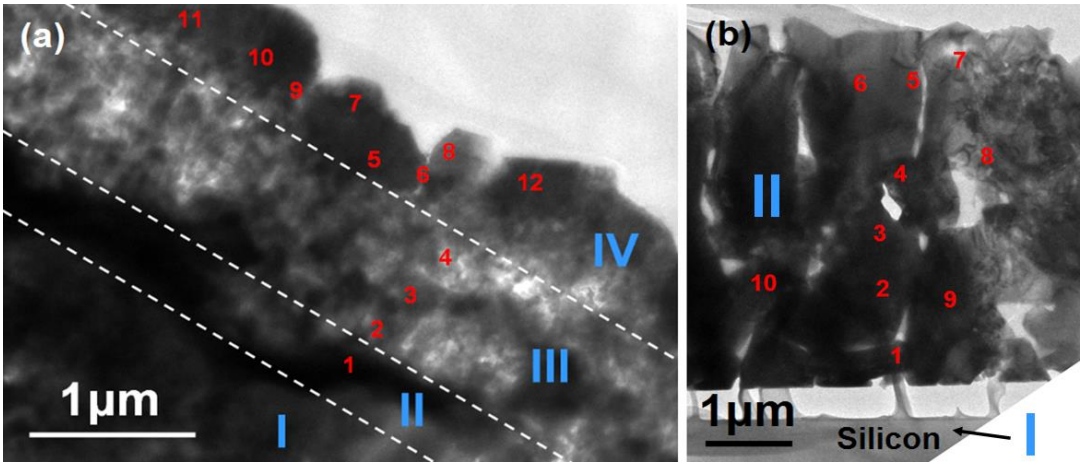

FIG 3. (a) TEM micrograph of porous GaN layer doped with Mg grown on a Si(100) substrate obtained when a high concentration of Mg_3N_2 was used. Each of the 4 layers indicated in Fig. 1 are marked. (b) TEM micrograph of the porous GaN layer doped with Mg on a Si(100) substrate obtained using a low concentration of Mg_3N_2

Position #	Mg %	Ga %	Position #	Mg %	Ga %
EDS content of Mg and Ga in the MOS diode layers					
1	73.3	26.7	7	11.7	97.8
2	98.5	1.5	8	7.9	92.1
3	97.0	3	9	9.5	90.5
4	97.3	2.7	10	8.9	91.1
5	7.9	92.1	11	7.9	92.1
6	11	89	12	8.1	91.9
EDS content of Mg and Ga in Mg-doped GaN					
1	1.3	98.7	6	2.2	97.8
2	1.5	98.5	7	2.5	97.6
3	1.9	98.1	8	1.8	98.2
4	3.9	96.1	9	1.8	98.2
5	2.6	97.4	10	1.4	98.6

TABLE 1. EDS content of Mg and Ga in the final MOS diode layers and Mg-doped GaN. The measurement points (#) relate to those numbered in Fig. 3.

The following mechanism is proposed for the uninterrupted CVD growth of the interfacial high-κ MgO layer on an Ohmic intermetallic with catalytic growth of GaN as a MOS diode, summarized in Fig. 1. Firstly, a intermetallic layer of Ga, Mg and the metallic catalyst (Au or Pt) used for a solid eutectic phase identified in region I in Figure 2, forms layer II. At higher temperatures a second layer formed almost entirely by Mg is deposited on the intermetallic layer. This layer quickly oxidizes to

polycrystalline MgO by reaction with O_2 when the furnace is opened, forming layer III. Finally, the growth of nanoporous GaN particles doped with Mg (layer IV) should proceed on the top of this Mg layer, acting Mg as a catalyst for the formation of this porous layer, since it appears not to be in contact with the catalyst with which we coated the substrate. Since no residual Mg, or MgO is found on the unintentionally n-doped GaN after heating and exposure to oxygen when the furnace was opened, the growth of the porous GaN particles proceeds through the Vapor-Solid-Solid (VSS) mechanism, consistent with that observed without the deposition of the Mg-containing material[28].

Figure 4 shows the *I-V* curves from the porous GaN catalyzed by Au (forming Ga_2Au). The *I-V* curves show only slight asymmetry indicative of near ohmic, weak Schottky barriers. Consistently, the conductivity of porous GaN grown from Pt was separately shown to be higher than that grown from Au[28]. The intermetallic layer contacts are described using the thermionic emission theory, taking into account a high ideality factor for weak barriers. The Schottky barrier height $\varphi_{B,n}^{o}$ (SBH) is estimated from $I = I_0 \exp[(qV - IR_s)/kT\ - 1]$ with $I_0 = AA^{**}T^2 \exp(-q\varphi_{B,n}^{o}/kT)$ where A^{**} is the effective Richardson constant (26.4 A cm^{-2} K^{-2})[45]. The estimated SBHs for Au-catalysed porous n-GaN to be 0.66 eV. It is worth noting that the n-type contacts were effectively ohmic as deposited and did not need any post-deposition annealing to induce this effective ohmicity. For porous GaN, and also for GaN grown on Mg-based films, the effect of an interfacial oxide was considered. The barrier height of an untreated metal/GaN diode can be altered by (photo)electrochemical etching treatment that leave defective GaN surface and interfaces, and described according to $\varphi_{B,n} = \varphi_{B,n}^{0} + \Delta\varphi$ where $\varphi^{0}{}_{B,n}$ represents the barrier height without the interfacial layer and $\Delta\varphi$ is the additional barrier due to the oxide. The parameter $\Delta\varphi$ is considered like a tunneling barrier of the form $\Delta\varphi = \frac{2kT}{\hbar}(2m\chi)^{\frac{1}{2}}\delta$ where h is Plank's

constant, m is the tunneling effective mass, χ is the mean tunneling barrier and δ is the thickness of the interfacial oxide. $\Delta\varphi$ was found to be in the range 0.18 – 0.25 eV for Pt and Au based intermetallic contacts to n-GaN[28]. This corresponds to a maximum native oxide thickness of ~2.7 nm on untreated GaN and would increase the overall effective barrier height. Microscopy and transport measurements thus confirm the porous catalyzed GaN growth is mostly free of influential surface contaminants.

The MgO-GaN porous layers formed on silicon exhibit diode behavior consistent with a MOS system. Figure 4 shows *I-V* curves across the device using an In-Ga euctectic to ohmically contact both the silicon substrate and the porous GaN. A rectifying diode response is found in the presence of the MgO, compared to ohmic response between the intermetallic termination porous n-GaN and the substrate. We assumed that the net current is due to thermionic emission current since the metal-semiconductor-metal contact now contains a dielectric at one interface, mimicking a Schottky contact with series resistance and an interfacial layer. Additionally, this is confirmed by forward bias voltages of $V > 3kT/q$, which is the case for this MOS diode. The downturn to linearity in the current after ~0.25 V confirms a series resistance, R_S, most likely originates from the MgO and porous n-GaN, as opposed to either of the metal contacts which are confirmed to be ohmic in nature. At higher bias (>0.25 V), the R_S dominates, as can be seen from the differential conductance dI/dV curve in Fig. 4a.

Effective ohmic contacts can form with n-type GaN suggesting that the resistivity dominates transport through an alloyed interface that promotes ohmic transport.[28] When a high-κ MgO layer is introduced, the series resistance markedly increases at much lower voltages. The MgO/n-GaN sandwich effectively has an altered electron affinity with respect to the In-Ga top contact. The overall series resistance, R_S, to which the sheet and contact resistivities contribute can also be determined from diffusion and thermionic emission theory summarised for a barrier-

dominated diode. For the Ga_2Au intermetallic contact, the response in Fig. 4b is symmetric (Ohmic). The current system behaves as a diode but utilizing an Ohmic contact formed by the intermetallic under the MgO layer, biased by the underlying silicon substrate. In the presence of the intermetallic bottom contact, the transport is effectively ohmic at the MgO interface. As the top contact to n-GaN is also Ohmic, the diodic response in Fig. 4b is dominated from affinity differences between the MgO and the n-GaN (doped at ~10^{16} cm^{-3}). The series resistance can also be obtained from the differential resistance through its proportionality to the current according to

$$\frac{dV}{dI} = \left(R_s + \frac{kT}{q}\left[\frac{1/I_0}{I/I_0 - 1}\right]\right) \approx R_s + \frac{nkT}{qI} \qquad (1)$$

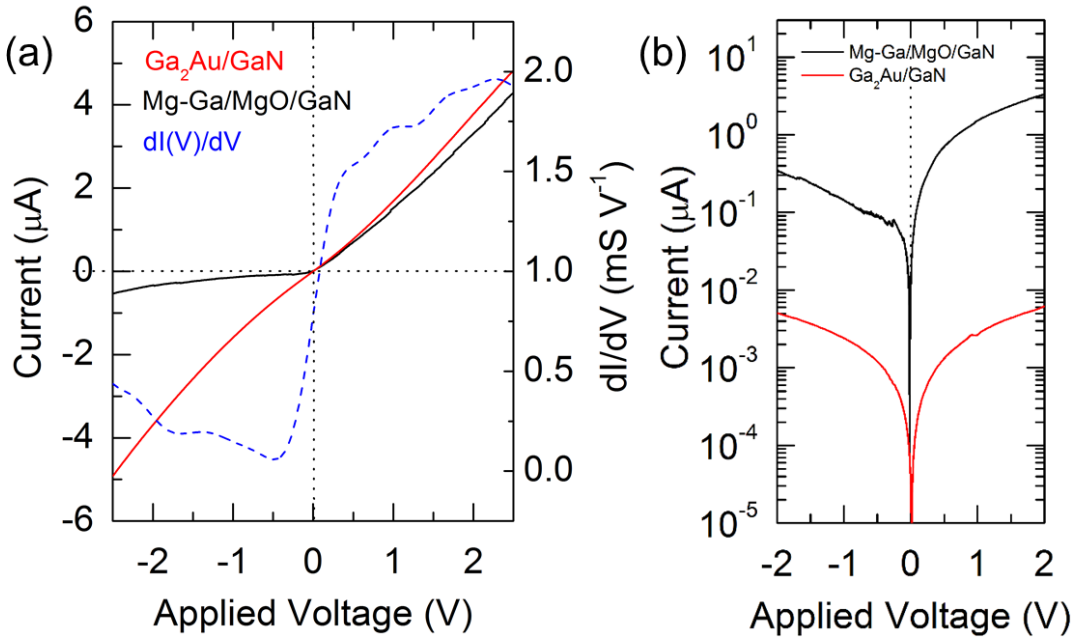

FIG 4. (a) *I-V* and d*I*/d*V* curves for porous n-GaN with a MgO dielectric layer, and from a Au-seeded porous GaN layer on silicon. (b) ln(*I*)-*V* curve for the ohmic Au-seeded GaN contact and the MgO-GaN diode.

Figure 5a shows the differential resistance d*V*/d*I* as a function of the inverse of the current, plotted according to Eq. 1. Although it does not allow deconvolution of the specific grain boundary resistance contribution to current flow through the porous layers, the series resistance is estimated to be in the range 5-6 kΩ for the MgO/porous GaN sandwich; d*V*/d*I* approaches R_S at the higher currents, but as seen in Fig. 5b, the

series resistance also includes likely tunnelling effects as the ideality factor is strongly voltage dependent and quite high in the higher current and higher bias regions. Further work is underway to identify the mechanism contributing to such high ideality factors, which are indicative of several mechanisms including tunnelling current through multiple heterojunctions. Porosity complicates the transport mechanism, increasing shunt and series resistances[46]. One possibility is a strong contribution by Poole–Frenkel (P-F) tunneling, and surface leakage. In the former, electron-hole transport processes are accommodated by lowering of the barrier when the carriers interact with the trap states in the MgO layer, especially since electron microscopy confirms that its morphology is not continuous. These recombinative states are likely to have a high density in a thick MgO film with a graded MgO composition at the interface with GaN (lower) and also with the silicon substrate (higher Mg concentration), as determined by elemental concentrations within the MgO layer at either interface. Variations in the interfacial composition is known to strongly affect Schottky and P-F leakage current in MOS structures[47].

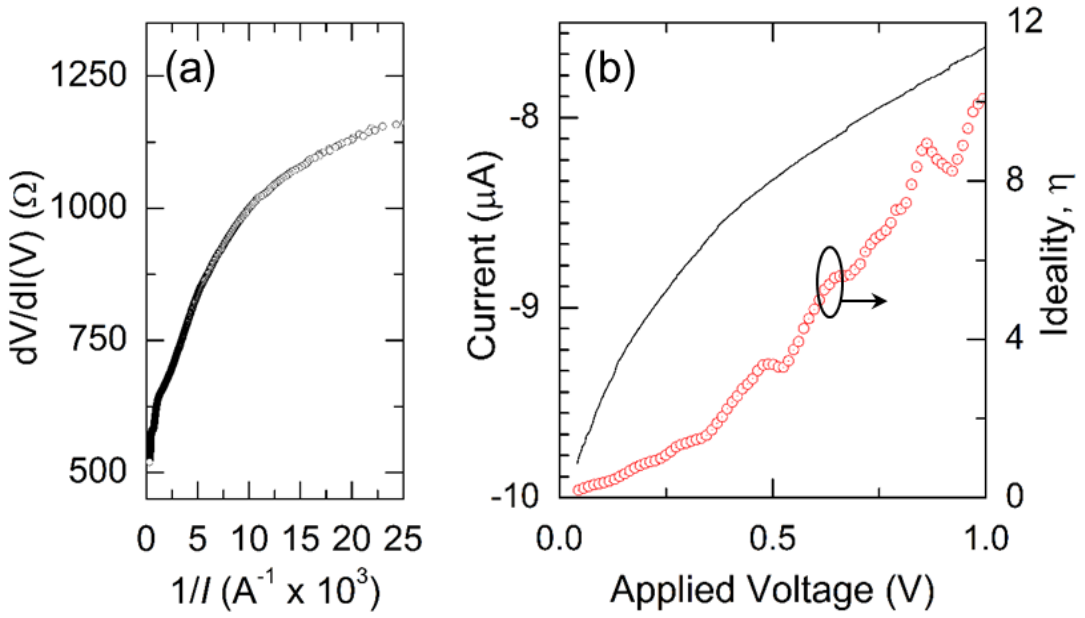

FIG 5. (a) Differential resistance (d*V*/d*I*) as a function of current for the MgO/porous GaN diode. (b) ln(*I*)-*V* curve and the voltage dependence of the ideality factor for the diode.

Thus, charge transport measurements through this system were conducted using 2- and 4-probe measurements and confirm the fabrication of a porous GaN diode, catalyzed by Mg that subsequently undergoes oxidative crystallization to form a MgO high-κ dielectric layer. The MOS diode-like response was confirmed through composition, microscopy and electrical transport analyses. Ohmic transport is found in the absence of a second oxide semiconducting layer between the intermetallic and the porous n-GaN. The porous GaN layer retains a similar morphology and conduction type to porous GaN catalyzed using Au or Pt on silicon. The method may be extended to growing nanoscale III-N materials and alloys using metals that are not typically employed for contacting, to give ohmic response and MOS-based systems on silicon substrates for chemically inert, high surface area electrically continuous transistors and diodes for capacitive (bio)sensing.

Conclusions

In summary, porous GaN crystals have been successfully grown as high surface area layers from Pt- and Au-coated silicon substrates by a vapor-solid-solid process. The particles form as a layer of single-crystal particles with interparticle and intraparticle porosity. Current-voltage and capacitance-voltage measurements show near-ohmic transport through low-doped, polycrystalline (as a layer), porous n-GaN without alloy contacts or low work function metals. Metal-Ga intermetallic alloy formation during vapor-solid-solid growth promotes thermionic emission-based low-resistance ohmic transport through the porous layer and very low contact resistivity is possible to the faceted, rough n-GaN surface. By depositing Mg in a manner similar to deterministic p-type doping of GaN, a similar porous GaN is formed. The Mg films is subsequently oxidized to polycrystalline MgO underneath the porous n-GaN layer, resulting in a high-κ dielectric oxide that allows the single step formation of a porous GaN/MgO MOS diode. The development of porous GaN augers well for new electronic and

optoelectronic devices with improved external quantum efficiencies, the incorporation of phosphors for LEDs, and high surface area biosensing based on capacitor or transistor function.

Acknowledgements

This project was supported by the EU Framework 7 under Project No. FP7-SPA-2010-263044, the Spanish Government under Projects No. MAT2011-29255-C02-02, TEC2010-21574-C02-02, and by Catalan Authority under Project No. 2009SGR235. This work was also supported by the UCC Strategic Research Fund, and through the Irish Research Council New Foundations Award 2012. A.V-C and P.R. acknowledge the EU under the Grant Agreement No. PITN-GA-2008-213238, Initial training network RAINBOW of the 7 RTD Framework.

References

1. Nakamura, S.; Pearton, S.; Fasol, G., *The blue laser diode: the complete story*. Springer-Verlag: Berlin Heidelberg, 2000.
2. Huang, Y.; Duan, X.; Cui, Y.; Lieber, C. M., *Nano Lett.* **2002,** *2*, 101−104.
3. Song, J. O.; Ha, J.-S.; Seong, T.-Y., *IEEE Electron. Dev. Lett.* **2010,** *57*, 42.
4. Yang, Y.; Ling, Y.; Wang, G.; Lu, X.; Tong, Y.; Li, Y., *Nanoscale* **2013,** *5*, 1820-1824.
5. Yang, C.-C.; Lin, C. F.; Lin, C.-M.; Chang, C. C.; Chen, K.-T.; Chien, J.-F.; Chang, C.-Y., *Applied Physics Letters* **2008,** *93*, 203103-203103-3.
6. Pearton, S. J.; Lele, T.; Tseng, Y.; Ren, F., *Trends in Biotechnology* **2007,** *25*, 481.
7. Lo, C.-F.; Xia, Y.; Liu, L.; Pearton, S. J.; S. Doré; Hsu, C.-H.; Dabiran, A. M.; Chow, P. P.; Ren, F., *Sensors and Actuators B* **2013,** *176*, 708.
8. Li, Y.; Xiang, J.; Qian, F.; Gradecak, S.; Wu, Y.; Yan, H.; Lieber, C. M., *Nano Lett.* **2006,** *6*, 1468.
9. Zhong, Z.; Qian, F.; Wang, D.; Lieber, C. M., *Nano Lett.* **2003,** *3*, 343.
10. Li, Y.; Qian, F.; Xiang, J.; Lieber, C. M., *Materials Today* **2006,** *9*, 18.
11. Qian, F.; Li, Y.; Gradecak, S.; Park, H.-G.; Dong, Y.; Ding, Y.; Wang, Z. L.; Lieber, C. M., *Nat. Mater.* **2008,** *7*, 701.
12. Qian, F.; Li, Y.; Gradecak, S.; Wang, D.; Barrelet, C. J.; Lieber, C. M., *Nano Lett.* **2004,** *4*, 1975.
13. Cullis, A. G.; Canham, L. T., *Nature* **1991,** *353*, 335.
14. McSweeney, W.; Lotty, O.; Mogili, N. V. V.; Glynn, C.; Geaney, H.; Tanner, D.; Holmes, J. D.; O'Dwyer, C., *J. Appl. Phys.* **2013,** *114*, 034309.
15. Hochbaum, A. I.; Gargas, D.; Hwang, Y. J.; Yang, P., *Nano Lett.* **2009,** *9*, 3550.
16. Lynch, R.; O'Dwyer, C.; Quill, N.; Nakahara, S.; Newcomb, S. B.; Buckley, D. N., *J. Electrochem. Soc.* **2013,** *160*, D260-D270.

17. Wang, Y. D.; Chua, S. J.; Sander, M. S.; Chen, P.; Tripathy, S.; Fonstad, C. G., *Applied Physics Letters* **2004,** *85*, 816-818.
18. Diaz, D. J.; Williamson, T. L.; Adesida, I.; Bohn, P. W.; Molnar, R. J., *J. Appl. Phys.* **2003,** *94*, 7526-7534.
19. Bardwell, J. A.; Foulds, I. G.; Webb, J. B.; Tang, H.; Fraser, J.; Moisa, S.; Rolfe, S., *J. Electron. Mater.* **1999,** *28*, L24-L26.
20. Huber, F.; Lang, H. P.; Gerber, C., *Nat. Nanotechnol.* **2008,** *3*, 645-646.
21. Chen, R. J.; Bangsaruntip, S.; Drouvalakis, K. A.; Kam, N. W. S.; Shim, M.; Li, Y.; Kim, W.; Utz, P. J.; Dai, H., *Proc. Natl. Acad. Sci.* **2003,** *100*, 4984.
22. Sandhu, A., *Nat. Nanotechnol.* **2007,** *2*, 746-748.
23. Pearton, S. J.; Norton, D. P.; Ren, F., *Small* **2007,** *3*, 1144.
24. Lo, C.-F.; Liu, L.; Chu, B.-H.; Ren, F.; Pearton, S. J.; Dore, S.; Hsu, C.-H.; Kim, J.; Dabiran, A. M.; Chow, P. P., *J. Vac. Sci. Technol. A: Vacuum, Surfaces, and Films* **2012,** *B30*, 010606-1-4.
25. Wang, Y.-L.; Chu, B. H.; Chang, C. Y.; Lo, C. F.; Pearton, S. J.; Dabiran, A.; Chow, P. P.; Ren, F., *Sensors and Actuators B* **2010,** *146*, 349.
26. Lo, C.-F.; Chu, B. Y.; Pearton, S. J.; Dabiran, A.; Chow, P. P.; Dore, S.; Hung, S. C.; Chen, C. W.; Ren, F., *Appl. Phys. Lett.* **2011,** *99*, 142107.
27. Pearton, S. J.; Ren, F., *Adv. Mater.* **2000,** *12*, 1571.
28. Bilousov, O. V.; Carvajal, J. J.; Drouin, D.; Mateos, X.; Díaz, F.; Aguiló, M.; O'Dwyer, C., *ACS Appl. Mater. Interfaces* **2012,** *4*, 6927-6934.
29. Bilousov, O. V.; Geaney, H.; Carvajal, J. J.; Zubialevich, V. Z.; Parbrook, P. J.; Giguère, A.; Drouin, D.; Díaz, F.; Aguiló, M.; O'Dwyer, C., *Appl. Phys. Lett.* **2013,** *103*, 112103.
30. Persson, A. I.; Larsson, M. W.; Stenstron, S.; Ohlsson, B. J.; Samuelson, L.; Wallenberg, L. R., *Nat. Mater.* **2004,** *3*, 677.
31. Ramizy, A.; Hassan, Z.; Omar, K., *Sens. Actuators B: Chemical* **2011,** *155*, 699-708.
32. Duan, B. K.; Bohn, P. W., *Analyst* **2010,** *135*, 902-907.
33. Yan, L.; Lopez, C. M.; Shrestha, R. P.; Irene, E. A.; Suvorova, A. A.; Saunders, M., *Appl. Phys. Lett.* **2006,** *88*, 142901.
34. Gila, B. P.; Kim, J.; Luo, B.; Onstine, A.; Johnson, W.; Ren, F.; Abernathy, C. R.; Pearton, S. J., *Solid-State Electron.* **2003,** *47*, 2139.
35. Carvajal, J. J.; Rojo, J. C., *Cryst. Growth Des.* **2009,** *9*, 320.
36. Carvajal, J. J.; Bilousov, O.; Drouin, D.; Aguiló, M.; Díaz, F.; Rojo, J. C., *Microsc. Microanal.* **2012,** *18*, 1.
37. Vermaut, P; Ruterana, P.; Nouet, G.; Morkoç, H., *Inst. Phys. Conf. Ser.* **1995**, *146*, 289
38. Ning, X.J.; Chien, F.R.; Pirouz, P.; Wang, J.W.; Khan, M.A, *J. Mater. Res.* **1996**, *3*, 580
39. Potin, V.; Nouet, G.; Ruterana, P., *Phil. Mag. A* **1999**, *79*, 2899
40. Ruterana, P.; Barbaray, B.; Béré, A.; Vermaut, P.; Hairie, A.; Paumier, E.; Nouet, G.; Salvador, A.; Botchkarev, A.; Morkoc, H., *Phys. Rev. B* **1999**, *59*, 1591
41. Potin, V.; Ruterana, P.; Nouet, G., *J. Phys. Condensed Matter* **2000**, *12*, 10301
42. Ruterana, P.; Potin, V.; Barbaray, B.; Nouet, G., *Phil. Mag. A* **2000**, *80*, 937
43. Sánchez, A.M.; Ruterana, P.; Benamara, M.; Strunk,H.P., *Appl. Phys. Lett.* **2003**, *82*, 4471
44. Potin, V.; Ruterana, P.; Nouet, G.; Pond, R.C.; Morkoç, H., *Phys. Rev. B* **2000**, *61*, 5587
45. Schroder, D. K., *Semiconductor Material and Device Characterization*. Wiley: New York, 1998.

46. Franssen, G.; Litwin-Staszewska, E.; Piotrzkowski, R.; Suski, T.; Perlin, P., *J. Appl. Phys.* **2003,** *9*, 6122
47. Tsao, H.-Y.; Lin, Y.-J.; Chen, Y.-H.; Chang, H.-C., *Solid State Commun.* **2011,** *151*, 693-696.

TOC Graphic